

# Constraints on the outer radius of the broad emission line region of active galactic nuclei

Hermine Landt<sup>1\*</sup>†, Martin J. Ward<sup>1</sup>†, Martin Elvis<sup>2</sup>† and Margarita Karovska<sup>2</sup>

<sup>1</sup>*Department of Physics, Durham University, South Road, Durham, DH1 3LE*

<sup>2</sup>*Harvard-Smithsonian Center for Astrophysics, 60 Garden Street, Cambridge, MA 02138, USA*

Accepted . Received ; in original form

## ABSTRACT

Here we present observational evidence that the broad emission line region (BELR) of active galactic nuclei (AGN) generally has an outer boundary. This was already clear for sources with an obvious transition between the broad and narrow components of their emission lines. We show that the narrow component of the higher-order Paschen lines is absent in *all* sources, revealing a broad emission line profile with a broad, flat top. This indicates that the BELR is kinematically separate from the narrow emission line region. We use the virial theorem to estimate the BELR outer radius from the flat top width of the unblended profiles of the strongest Paschen lines, Pa $\alpha$  and Pa $\beta$ , and find that it scales with the ionising continuum luminosity roughly as expected from photoionisation theory. The value of the incident continuum photon flux resulting from this relationship corresponds to that required for dust sublimation. A flat-topped broad emission line profile is produced by both a spherical gas distribution in orbital motion as well as an accretion disc wind if the ratio between the BELR outer and inner radius is assumed to be less than  $\sim 100 - 200$ . On the other hand, a pure Keplerian disc can be largely excluded, since for most orientations and radial extents of the disc the emission line profile is double-horned.

**Key words:** galaxies: active – galaxies: nuclei – infrared: galaxies – quasars: emission lines

## 1 INTRODUCTION

The broad emission line region (BELR) of active galactic nuclei (AGN) is one of the most direct tracers of the immediate environment of supermassive black holes. However, despite decades of intensive optical and ultraviolet (UV) spectrophotometric studies its geometry and kinematics remain ill-defined. It is not clear whether the BELR gas has a spherical, bi-conical or disc-like distribution, and whether it consists of a large number of discrete clouds (e.g. Mathews 1974; Krolik et al. 1981; Emmering et al. 1992; Baldwin et al. 1995) or is part of an outflowing, continuous gas distribution such as an accretion disc wind (e.g. Murray et al. 1995; Murray & Chiang 1997). The knowledge of the BELR geometry and kinematics is essential not only to our understanding of the relationship between different

types of AGN but in particular to studies that estimate black hole masses from the widths of the broad emission lines. These estimates would not be meaningful if the BELR gas kinematics were dominated by radial motion, and if the gas was gravitationally bound but distributed in a disc, the resulting values would be underestimated for sources viewed face-on.

Our current, limited knowledge of the BELR physical conditions and scales was gained primarily through the application of photoionisation models to the observed emission line intensities and ratios (see, e.g., review by Ferland 2003) and through reverberation mapping studies of the (correlated) continuum and line variability (see, e.g., review by Peterson 1993). Both of these methods have relied so far on spectroscopic observations at optical and UV frequencies, but investigating also the near-infrared (near-IR) wavelengths can offer several advantages. First, the near-IR broad emission lines are little reddened and, therefore, when compared to lines at higher frequencies, can yield information on the amount of dust extinction affecting the BELR. Secondly, since each emission line is formed most efficiently at a particular density and distance from the ionis-

\* E-mail: hermine.landt@durham.ac.uk

† Visiting Astronomer at the Infrared Telescope Facility, which is operated by the University of Hawaii under Cooperative Agreement no. NNX-08AE38A with the National Aeronautics and Space Administration, Science Mission Directorate, Planetary Astronomy Program.

ing source (Baldwin et al. 1995), it is important to incorporate in photoionisation and reverberation mapping studies multiple emission lines to map the entire BELR. In this respect, cross-dispersed near-IR spectra, which are now available at several observing sites, have a large wavelength coverage and so offer the unique opportunity to simultaneously observe a plethora of different emission lines. For example, in low-redshift sources, such spectra cover the wavelength region of  $\sim 16$  hydrogen lines from the Paschen and Brackett series, as well as that of several lines from other chemical species such as helium, oxygen, calcium and singly-ionised iron (Landt et al. 2008).

Finally, the near-IR broad emission lines trace in depth the low-ionisation line (LIL) region, a region believed to have extreme properties such as very high densities ( $n > 10^{11} \text{ cm}^{-3}$ ) and a disc-like structure (Collin-Souffrin & Lasota 1988; Marziani et al. 1996). However, these properties were derived mainly based on observations of the two Balmer lines,  $H\alpha$  and  $H\beta$ , which are strongly blended with other species. Since the crucial measurements for these studies are the emission line flux and profile a verification of the results using *unblended* broad emission lines is needed. As we have shown in Landt et al. (2008), the profiles of the strongest Paschen lines,  $\text{Pa}\alpha$  and  $\text{Pa}\beta$ , are observed to be unblended and, therefore, are well-suited to test BELR models. However, in order to do so in a meaningful way one needs to first isolate the profile of the broad component from that of the narrow emission line region (NELR), which is not a straightforward task in sources where the broad emission lines are relatively narrow and so the narrow and broad components smoothly merge into each other.

Here we present observational evidence that the BELR of *all* AGN has an outer boundary, which means that it is kinematically separate from the NELR. The paper is organised as follows. In Section 2, we briefly introduce the sample and discuss the data. In Section 3, based on the higher-order Paschen lines, we show that the intrinsic BELR profile has a broad, flat top, which indicates an outer radius. In Section 4, we estimate the BELR outer radius from the flat top width of the unblended profiles of the strongest Paschen lines,  $\text{Pa}\alpha$  and  $\text{Pa}\beta$ , using the virial theorem and investigate if the BELR is dust-limited. In Section 5, we discuss BELR models in the light of their ability to produce a flat-topped profile. Finally, in Section 6, we summarise our main results and present our conclusions. Throughout we have assumed cosmological parameters  $H_0 = 70 \text{ km s}^{-1} \text{ Mpc}^{-1}$ ,  $\Omega_M = 0.3$ , and  $\Omega_\Lambda = 0.7$ .

## 2 THE SAMPLE AND DATA

The target selection, observational strategy, and data reduction procedures for our original sample have been described in detail in Landt et al. (2008). In short, we obtained for 23 relatively nearby ( $z \lesssim 0.3$ ) and bright ( $J \lesssim 14$  mag) broad emission line AGN during four observing runs contemporaneous (within two months) near-IR and optical spectroscopy. The observations were carried out between 2004 May and 2007 January with a single object being typically observed twice within this period. The near-IR spectra were obtained with the SpeX spectrograph (Rayner et al. 2003) at the NASA Infrared Telescope Facility (IRTF), a 3 m telescope

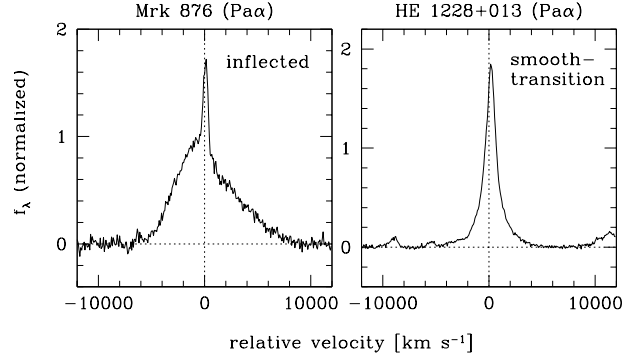


**Figure 1.** Observed  $\text{Pa}\alpha$  emission lines in velocity space relative to the expected rest-frame wavelength. The separation between the broad and narrow line components is obvious when the profile has an inflection (left panel), but not so when the emission lines are relatively narrow and the broad and narrow line components smoothly transition into each other (right panel).

on Mauna Kea, Hawai'i. We chose the short cross-dispersed mode (SXD,  $0.8 - 2.4 \mu\text{m}$ ) and a slit of  $0.8 \times 15''$ , which resulted in an average spectral resolution of full width at half-maximum (FWHM)  $\sim 400 \text{ km s}^{-1}$ . In Landt et al. (2008), we presented the data of the first three epochs (2004 May, 2006 January, and 2006 June) and in Landt et al. (2011b) we added the fourth epoch (2007 January).

We obtained near-IR spectroscopy for an additional sample of nine broad emission line AGN in order to improve the calibration of the near-IR relationship for estimating black hole masses presented in Landt et al. (2011a). Details on the target selection, observational strategy, and data reduction procedures can be found in Landt et al. (2013). In short, we observed in queue mode at the *Gemini* North observatory, an 8.1 m telescope on Mauna Kea, Hawai'i, with the Gemini Near-Infrared Spectrograph (GNIRS; Elias et al. 2006) in its Science Verification (SV) phase and in semester 2011B. We used the cross-dispersed mode with the short camera ( $0.9 - 2.5 \mu\text{m}$ ) and a slit of  $0.675 \times 7''$ . This set-up gives an average spectral resolution of FWHM  $\sim 400 \text{ km s}^{-1}$ , similar to that of the IRTF near-IR spectra.

All spectra have relatively high continuum signal-to-noise (S/N) ratios ( $\gtrsim 100$ ), which allows us to study even the weakest lines in the Paschen series and to interpret the profiles of the strongest Paschen lines,  $\text{Pa}\alpha$  and  $\text{Pa}\beta$ , with high confidence. In the case of the IRTF data, we have used for our main analysis only the highest-quality spectrum. Furthermore, we have excluded the source Mrk 590, since it was found to be in a very low AGN state with weak and noisy broad emission lines. Our total sample consists of 31 sources, for which we list in Table 1 the relevant measurements for the broad components of the  $\text{Pa}\alpha$  or  $\text{Pa}\beta$  emission lines, whichever had the higher S/N ratio. In the following, we assume that these broad components are representative of the hydrogen BELR and refer to them as 'template profiles'.

The profiles of the total observed  $\text{Pa}\alpha$  or  $\text{Pa}\beta$  emission lines of our sources fall roughly into two subclasses depending on the transition between the broad and narrow line components. The separation between the two components is obvious when the total profile has an inflection

**Table 1.** Parameters of the Paschen broad emission line region

Object Name	$z$	line	type	top width [km/s]	$M_{\text{BH}}$ [ $M_{\odot}$ ]	Ref.	$R_{\text{H}\beta}$ [lt-days]	Ref.	$R_{\text{out}}$ [lt-days]	$\log \nu L_{\text{tot}}$ [erg s $^{-1}$ ]	$T_{\text{dust}}$ [K]	$R_{\text{dust}}$ [lt-days]
(1)	(2)	(3)	(4)	(5)	(6)	(7)	(8)	(9)	(10)	(11)	(12)	(13)
IRAS 1750+508	0.300	Pa $\beta$	e	884	3.3e+08	est	109	est	8604	47.07	1383	6556
H 1821+643	0.297	Pa $\beta$	i	2050	1.9e+09	est	253	est	9487	47.22	1320	8796
PDS 456	0.184	Pa $\beta$	e	998	8.0e+08	est	231	est	16382	47.41	1425	8972
3C 273	0.158	Pa $\beta$	e	1080	8.9e+08	P04	307	B09	15551	47.59	1443	10683
PG 0052+251	0.155	Pa $\alpha$	i	1523	3.7e+08	P04	90	B09	3260	46.07	1198	3012
PG 1307+085	0.155	Pa $\alpha$	i	729	4.4e+08	P04	106	B09	16950	46.22	1307	2854
PG 0026+129	0.145*	Pa $\alpha$	e	684	3.9e+08	P04	111	B09	17199	46.41	1127	5221
Mrk 876	0.129	Pa $\alpha$	i	877	2.8e+08	P04	40	B09	7441	46.22	1339	2680
HE 1228+013	0.117	Pa $\alpha$	e	865	1.0e+08	est	53	est	2829	46.67	1333	4552
PG 0804+761	0.100	Pa $\alpha$	lack	505	6.9e+08	P04	147	B09	55723	45.97	1314	2111
PG 1211+143	0.081	Pa $\alpha$	e	764	1.5e+08	P04	94	B09	5122	46.22	1337	2691
PG 0844+349	0.064	Pa $\alpha$	lack	651	9.2e+07	P04	32	B09	4472	46.18	1190	3478
Mrk 1513	0.063	Pa $\alpha$	e	801	4.6e+07	G12	10	G12	1470	46.33	1356	2944
3C 390.3	0.056	Pa $\alpha$	i	1478	1.3e+09	D12	44	D12	11810	44.95	1462	494
Mrk 110	0.035	Pa $\beta$	e	747	2.5e+07	P04	26	B09	923	46.00	1452	1685
Mrk 509	0.034	Pa $\beta$	e	1125	1.4e+08	P04	80	B09	2314	45.77	1398	1427
Ark 120	0.033	Pa $\beta$	lack	2546	1.5e+08	P04	40	B09	474	45.45	1102	1833
3C 120	0.033	Pa $\beta$	i	679	6.7e+07	G12	26	G12	2978	45.28	1389	826
Mrk 817	0.031	Pa $\beta$	i	1610	4.3e+07	D10	14	D10	342	45.65	1401	1236
Mrk 290	0.030	Pa $\beta$	i	1426	2.4e+07	D10	9	D10	245	45.36	1353	969
H 2106–099	0.027	Pa $\beta$	e	969	4.4e+07	est	11	est	953	45.28	1342	903
Mrk 335	0.026	Pa $\beta$	e	945	2.5e+07	G12	14	G12	574	45.63	1308	1444
Ark 564	0.025	Pa $\beta$	e	764	1.7e+07	est	8	est	614	45.37	1202	1334
Mrk 79	0.022	Pa $\beta$	i	836	5.2e+07	P04	15	B09	1535	44.82	1364	510
NGC 5548	0.017	Pa $\beta$	i	3731	4.4e+07	D10	12	D10	65	44.58	1547	279
NGC 7469	0.016	Pa $\beta$	i	567	1.2e+07	P04	5	B09	777	45.28	1551	620
H 1934–063	0.011	Pa $\beta$	e	745	1.0e+07	est	5	est	370	45.07	1426	605
NGC 4593	0.009	Pa $\beta$	i	2777	9.8e+06	D06	4	B09	26	44.72	1380	441
NGC 3516	0.009	Pa $\beta$	lack	2728	3.2e+07	D10	12	D10	87	...	...	...
NGC 3227	0.004	Pa $\beta$	i	1046	7.6e+06	D10	4	D10	143	...	...	...
NGC 4151	0.003	Pa $\beta$	i	2272	4.6e+07	B06	7	B09	181	43.24	1328	89

The columns are: (1) object name; (2) redshift from the NASA/IPAC Extragalactic Database (NED), which we checked with narrow emission lines; (3) emission line used as a template profile; (4) type of transition between the broad and narrow emission line component, where i: inflected (i.e., transition is obvious), e: estimated (i.e., transition is estimated), and lack: absent narrow emission line component; (5) full width of the flat top of the broad component; (6) black hole mass (in solar masses); (7) reference for the black hole mass, where B06: Bentz et al. (2006), D06: Denney et al. (2006), D10: Denney et al. (2010), D12: Dietrich et al. (2012), P04: Peterson et al. (2004), G12: Grier et al. (2012) and est: estimated based on the relationship between black hole mass and near-IR virial product presented in Landt et al. (2013); (8) radius of the H $\beta$  broad-emission line region (in light-days); (9) reference for the H $\beta$  radius, where B09: Bentz et al. (2009), est: estimated based on the relationship between H $\beta$  radius and 1  $\mu\text{m}$  continuum luminosity presented in Landt et al. (2013), and the remainder as in column (7); (10) outer radius (in light-days) calculated from the *half* width of the flat top using the virial theorem; (11) total accretion disc luminosity; (12) blackbody temperature of the hot dust derived from near-IR spectral continuum fits; and (13) hot dust radius (in light-days) estimated from the total accretion disc luminosity in column (11) and the hot dust temperature in column (12) using eq. (1) of Mor & Netzer (2012) for a silicate dust grain composition.

\* We measure a redshift of  $z = 0.145$  from narrow emission lines, instead of  $z = 0.142$  listed in NED.

(as exemplified in Fig. 1, left panel), but not so when the emission lines are relatively narrow and the broad and narrow line components smoothly transition into each other (Fig. 1, right panel). In the following we refer to these two subclasses of sources as ‘inflected’ and ‘smooth-transition sources’, respectively. In our sample, the total observed profiles of 14/31 sources is inflected and that of 13/31 sources is of the smooth-transition type. A further four sources (PG 0804+761, PG 0844+349, Ark 120 and NGC 3516) clearly lack a Paschen narrow line component, since their profiles have a broad top. For the analysis in Section 4 we have grouped these four sources with the inflected ones. Fig. A1 and A2 show the template profiles separately for the inflected and smooth-transition sources. The three inflected

sources 3C 120, NGC 7469 and NGC 3227 have been included in Fig. A2 rather than in Fig. A1 since they have relatively narrow broad emission lines. In the next section, we discuss our novel method to separate the broad and narrow emission line components in smooth-transition sources.

### 3 ABSENT NARROW COMPONENTS

Since the first optical spectroscopy of AGN it was realised that not all broad emission line profiles are peaked but that some have a very broad, flat top (e.g., Osterbrock et al. 1975, 1976). The narrow emission line component would then sit on top of these very broad profiles or be outright

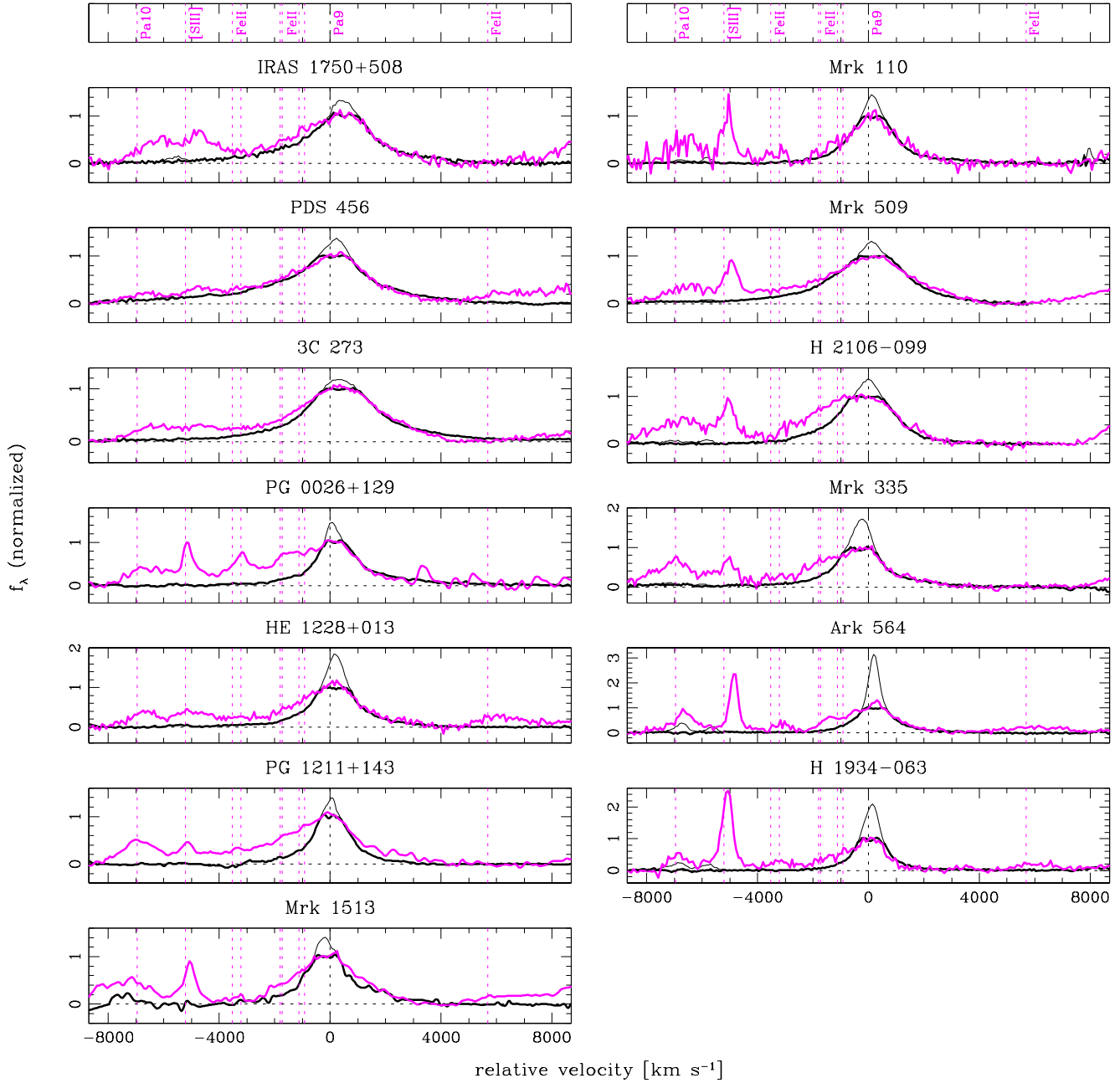


**Figure 2.** Observed profiles of the Pa9 and Pa10 emission lines (magenta) for the smooth-transition sources. The Pa9 profiles are compared to the template profiles (Pa $\alpha$  or Pa $\beta$ , black) in velocity space relative to the expected rest-frame wavelength. The absent Pa9 narrow component reveals a flat-topped broad emission line profile similar to that resulting for the template profiles (thick lines) after removing the largest possible flux contribution from the narrow emission line region (thin lines).

absent. In these AGN, it is evident that the BELR has an outer boundary and that it does not kinematically merge into the NELR. However, it is not immediately clear what the intrinsic broad emission line profile is when no flat top is observed and the total profile resembles rather that of a narrow emission line with a broad bottom and extended wings. In this section, we show that also in these AGN the broad emission line profiles are intrinsically flat-topped.

A crucial step towards isolating the intrinsic broad emission line profile in AGN is the subtraction of the narrow line component. This task is straightforward when the transition between the broad and narrow emission line components is obvious because there is a clear inflection in the profile, which is generally the case for broad components with FWHM a factor of  $\gtrsim 5$  larger than those of the narrow components (Landt et al. 2008). The profiles of roughly half

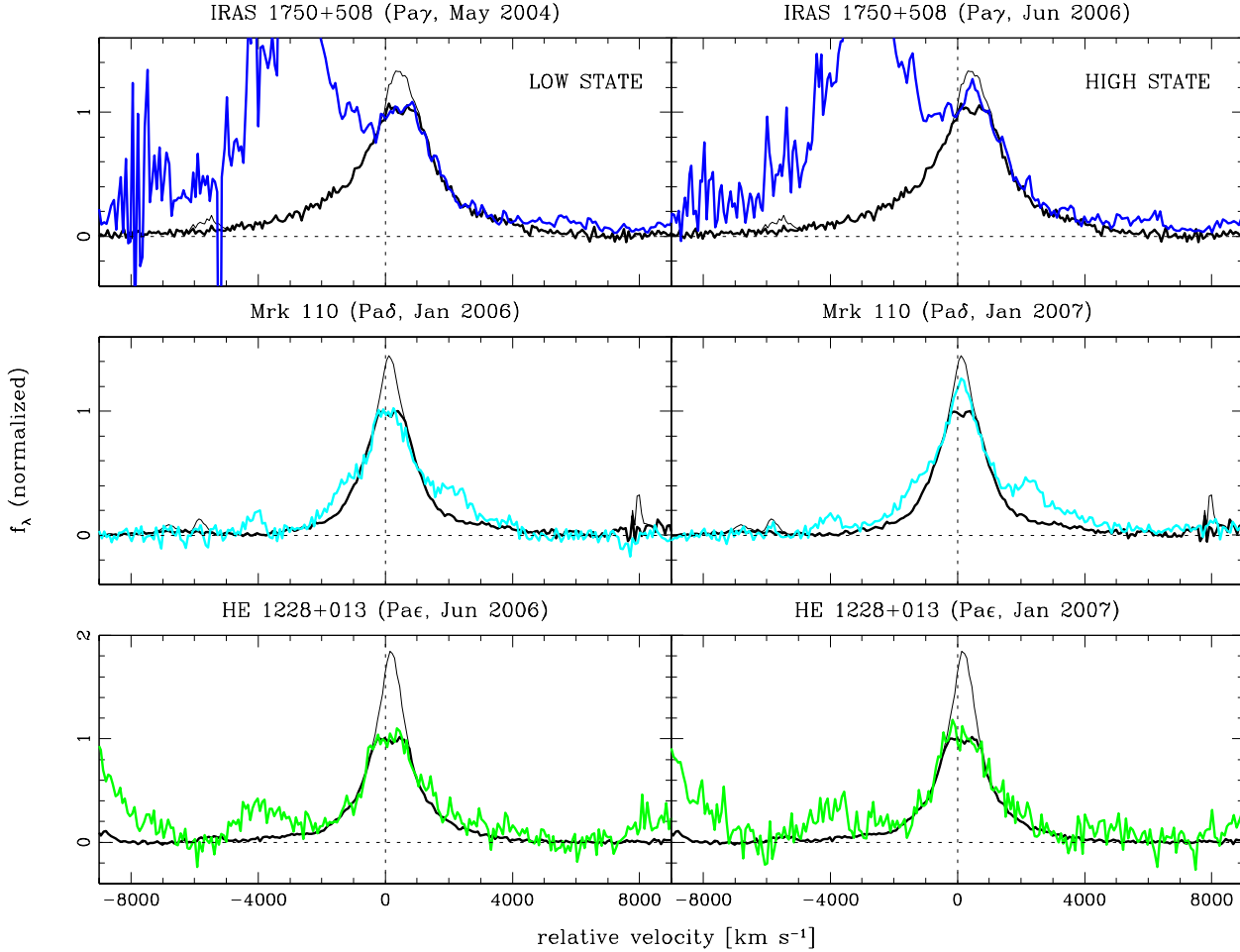


**Figure 3.** Observed profiles of the Pa $\gamma$  (blue), Pa $\delta$  (cyan) and Pa $\epsilon$  (green) emission lines for the smooth-transition sources IRAS 1750+508, Mrk 110 and HE 1228+013, respectively, compared to the template profiles (Pa $\alpha$  or Pa $\beta$ , black) in velocity space relative to the expected rest-frame wavelength. When the source is in a low flux state (left-hand panels), the absent Pa $\gamma$ , Pa $\delta$  and Pa $\epsilon$  narrow components reveal a flat-topped broad emission line profile. This profile is similar to that resulting for the template profiles (thick lines) after removing the largest possible flux contribution from the narrow emission line region (thin lines). When the source is in a high flux state (right-hand panels), the narrow component of the Pa $\epsilon$  emission line is absent in HE 1228+013, whereas the narrow components of the Pa $\gamma$  and Pa $\delta$  emission lines are present in IRAS 1750+508 and Mrk 110, respectively.

our sample fall in this category (exemplified in Fig. 1, left panel). When the broad emission lines are relatively narrow and the broad and narrow components smoothly transition into each other (see Fig. 1, right panel), two different approaches have been adopted so far to isolate the intrinsic broad emission line profile. The narrow component is assumed to be a Gaussian with FWHM the same as that of the forbidden narrow emission line [O III]  $\lambda$ 5007, which is taken to be representative of the NELR, and the flux of the Gaussian is either scaled to that of [O III]  $\lambda$ 5007 assuming Case B conditions (e.g. Marziani et al. 1996, 2003) or is fit for by modeling the entire emission line profile with the sum of two or three Gaussians (e.g. Zamfir et al. 2010; Jin et al. 2012). Both these methods yield an intrinsic broad emission line profile that is *peaked*. In Landt et al. (2008), we have taken yet a different approach and have fit in these cases a Gaussian with FWHM equal to that of [O III]  $\lambda$ 5007 to the *entire* top part of the total emission line profile. For the additional sample presented in Landt et al. (2013), for which

we did not have contemporaneous optical spectroscopy, we have used instead the FWHM of the near-IR narrow emission line [S III]  $\lambda$ 9531. Our new method assumes that the NELR and BELR are kinematically distinct and by scaling the flux of the Gaussian to the entire upper part of the emission line profile it subtracts the largest possible flux contribution from the NELR. Contrary to the other two methods, it yields an intrinsic broad emission line profile that is flat-topped, similar to what is observed in the inflected sources.

In support of our method, we present here a new finding; in *all* smooth-transition sources the narrow components of the higher-order Paschen emission lines, such as, e.g., Pa9 and Pa10 (Fig. 2), are absent. In some of these AGN, in particular when they are in a low flux state, we find absent narrow components even earlier in the Paschen series, e.g., Pa $\gamma$ , Pa $\delta$  and Pa $\epsilon$  for the sources IRAS 1750+508, Mrk 110 and HE 1228+013, respectively (Fig. 3). The absent narrow components reveal the intrinsic broad-line profile of the smooth-transition sources, which is observed to be flat-topped and

similar to both the profile that our method yields for the  $\text{Pa}\alpha$  and  $\text{Pa}\beta$  broad components and the Paschen broad-line profile of the inflected sources. The most likely reason for the absent narrow components of the higher-order Paschen emission lines is the much steeper flux decrement within the series for conditions prevalent in the NELR (i.e. for optically thin Paschen line emission) than for those typical of the BELR (i.e. for optically thick Paschen line emission). We note that the  $\text{Pa}\epsilon$  broad emission line is heavily blended with the strong narrow emission line  $[\text{S III}] \lambda 9531$  and, therefore, we cannot exclude that the  $\text{Pa}\epsilon$  narrow component is absent also in other sources. The source HE 1228+013 is the only one in our sample that lacks  $[\text{S III}] \lambda 9531$  emission. Furthermore, based on the observed flat-topped  $\text{Pa}9$  broad emission lines, we have now estimated the contribution of the narrow components to the template profiles also for the sources IRAS 1750+508 and PDS 456, which were left uncorrected by Landt et al. (2008).

#### 4 A DUST-LIMITED BELR

An intrinsically flat-topped broad emission line profile in *all* AGN indicates that the BELR generally has an outer radius. Next, we investigate if its value is set by the presence of dust, i.e. if the BELR is dust- rather than radiation-bounded. As Netzer & Laor (1993) have shown, when dust is present, the broad line emission diminishes sharply and narrow line emission is expected at much larger radii.

Assuming the gas dynamics are dominated by gravity, we have used the virial theorem  $M_{\text{BH}} = fR\Delta V^2/G$ , where  $M_{\text{BH}}$  is the black hole mass,  $R$  is the radial distance of the broad line gas,  $\Delta V$  is the gas velocity,  $G$  is the gravitational constant and  $f$  is the geometrical correction factor, to calculate the outer radius of the BELR. Half of the observed full width of the flat top readily gives  $\Delta V$ . We have measured the width of the flat top in the template profiles as indicated by the two vertical red dashed lines in Figs. A1 and A2. For the large majority of our sample (24/31 sources) we have black hole masses determined by optical reverberation mapping campaigns and for the remainder we have estimated this value based on our recently calibrated relationship between the black hole mass and the near-IR virial product (Landt et al. 2013). The geometrical correction factor  $f = 1$  in our case, since, contrary to the line dispersion or FWHM of the broad line, the outer radius and so the flat top width is independent of optical depth effects (Korista & Goad 2004). The results are listed in Table 1. We obtain BELR outer radii in the large range of  $R_{\text{out}} \sim 26$  lt-days – 153 lt-yrs.

In Fig. 4 (top panel), we first compare the resulting BELR outer radii to the radii of the  $\text{H}\beta$  broad line region obtained from reverberation mapping campaigns. For the seven sources without reverberation results we have estimated this value based on our recently calibrated relationship between the  $\text{H}\beta$  radius and the  $1 \mu\text{m}$  continuum luminosity (Landt et al. 2013). We expect the  $\text{H}\beta$  broad line gas at the largest radii to respond the strongest to changes in the ionising continuum flux, but at the same time emission line gas at smaller radii can respond more rapidly and more coherently than gas at larger radii, which will bias observed reverberation time lags towards smaller values (Korista & Goad 2000, 2004). Therefore, it is difficult to theoretically predict the

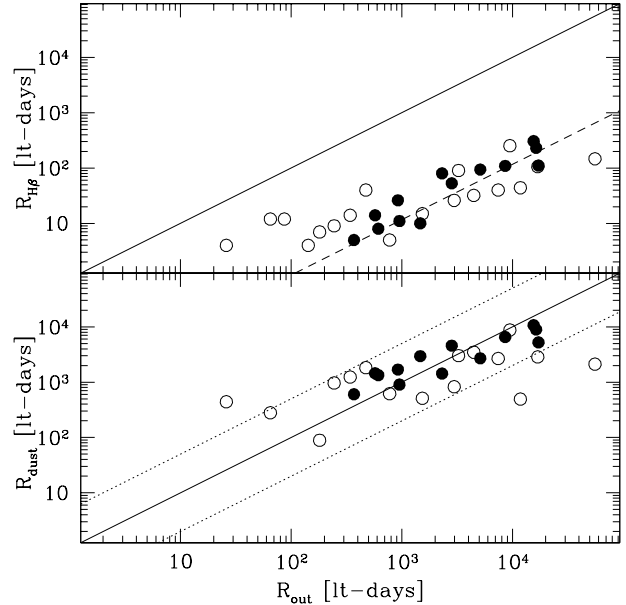


**Figure 4.** The reverberation radius of the  $\text{H}\beta$  broad line region (top panel) and the hot dust radius (calculated for a silicate dust grain composition; bottom panel) versus the BELR outer radius. Sources with template profiles ( $\text{Pa}\alpha$  or  $\text{Pa}\beta$ ) that have an obvious and an estimated transition between their broad and narrow components are shown as open and filled circles, respectively. In both panels we show the line of equality (solid line) with the dashed line indicating the mean for the entire sample of  $R_{\text{out}}/R_{\text{H}\beta} = 86$  (top panel) and the dotted lines showing the range of a factor of 5 around the line of equality (bottom panel).

expected ratio between the BELR outer radius and the reverberation radius and its empirical value can put important constraints on the covering fraction and radial density distribution of the line emitting gas. For our entire sample, we obtain a relatively large range of  $R_{\text{out}}/R_{\text{H}\beta} \sim 5 - 380$ , with a distribution mean of  $\langle R_{\text{out}}/R_{\text{H}\beta} \rangle = 86 \pm 15$  (dashed line) and a median value of  $R_{\text{out}}/R_{\text{H}\beta} = 54$ . The sources NGC 5548 and PG 0804+761 have the smallest and largest radius ratio, respectively. The large spread in values is mainly due to the inflected sources. If we consider the inflected and smooth-transition sources separately, the distribution means are  $\langle R_{\text{out}}/R_{\text{H}\beta} \rangle = 96 \pm 25$  and  $73 \pm 11$ , with corresponding median values of  $R_{\text{out}}/R_{\text{H}\beta} = 37$  and  $71$ , respectively. The much larger (a factor of  $\sim 2$ ) median value for the smooth-transition sources indicates that the gas emissivity, which strongly depends on the number density, in these sources does not drop as rapidly with radius as in the inflected sources, suggesting that they have much lower ionisation parameters. We will return to this point later in the section.

If the BELR is indeed dust-limited, we expect its emission to cease at a certain incident continuum photon flux, which should roughly coincide with that required for dust sublimation. On the other hand, the dust that possibly limits the BELR is most likely the same as the hot dust usually observed in the spectral energy distributions (SEDs) of broad emission line AGN, and so we expect a rough coincidence between the BELR outer radius and the average hot dust radius. In the following we search for these two

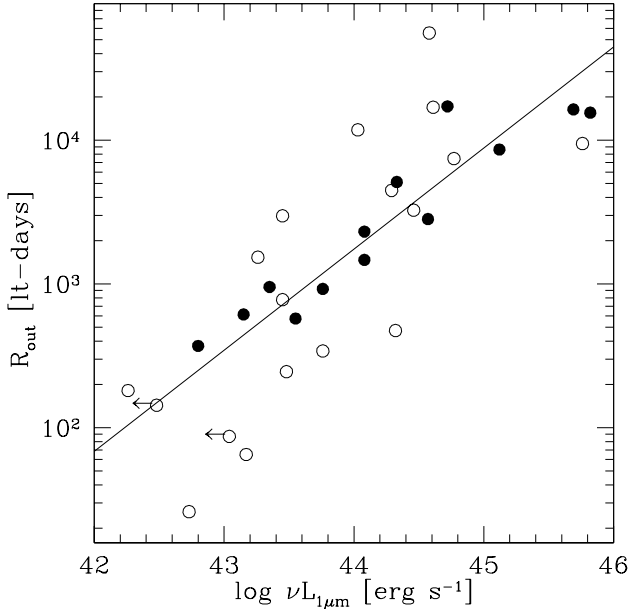


**Figure 5.** The outer radius (in light-days) versus the integrated  $1 \mu\text{m}$  continuum luminosity. Symbols are as in Fig. 4. The two sources with a continuum SED dominated by host galaxy emission are plotted as upper limits. The solid line indicates the observed correlation.

lines of evidence. First, in order to assess if there is a preferred ionisation flux that limits the BELR, we have plotted in Fig. 5 the radius-luminosity ( $R$ - $L$ ) relationship between the BELR outer radius and the integrated  $1 \mu\text{m}$  continuum luminosity. As we have shown in Landt et al. (2011b), the latter is dominated by the accretion disc spectrum, which is believed to be the main source of ionising radiation in AGN. The continuum SEDs of two of our sources (NGC 3516 and NGC 3227) are dominated by host galaxy emission and, therefore, their observed  $1 \mu\text{m}$  continuum luminosities represent only an upper limit to the AGN luminosity. Fig. 5 shows that there is a strong correlation between the BELR outer radius and the ionising luminosity. A least-squares fit (excluding the two upper limits) gives a correlation slope of  $0.7 \pm 0.1$ , which is consistent (within  $2\sigma$ ) with the value of  $0.5$  expected from simple photoionisation arguments. Therefore, it appears that the BELR in all AGN ceases at a similar ionising flux. Fig. 5 further supports our method for removing the narrow line components in smooth-transition sources. It shows that both the inflected and smooth-transition sources follow the same  $R$ - $L$  relationship, which means that we have not artificially introduced a broad, flat top in the latter. If that had been the case, for a given continuum luminosity, we would expect to find the smooth-transition sources at much lower BELR outer radii than those of the inflected sources.

Next, we have estimated the hot dust radius in our sources using the relationship between bolometric luminosity and dust sublimation temperature given by Mor & Netzer (2012). We have assumed that the dust sublimation temperature corresponds to the hot dust temperature and have derived the latter from blackbody fits to the near-IR spectral continuum as described in (Landt et al. 2011b). For our enlarged sample, the average hot dust

temperature is  $T_{\text{dust}} = 1347 \pm 20$  K, similar to our result in Landt et al. (2011b), which indicates a silicate dust grain composition. Therefore, we have used eq. (1) of Mor & Netzer (2012). We have approximated the bolometric luminosity with the total accretion disc luminosity, which we have obtained from spectral continuum fits as discussed in Landt et al. (2011b). Our results are listed in Table 1. Note that for two sources, namely, NGC 3516 and NGC 3227, we do not have an estimate of the hot dust radius since their near-IR spectra were found to be strongly dominated by host galaxy starlight (Landt et al. 2011b, 2013). In Fig. 4 (bottom panel), we compare the hot dust radii to the BELR outer radii. The distribution of the ratio between the two radii has a mean consistent with one ( $\langle R_{\text{dust}}/R_{\text{out}} \rangle = 1.9 \pm 0.6$ ) and a median value of  $R_{\text{dust}}/R_{\text{out}} = 0.8$ . As previously in Fig. 4 (top panel), the inflected sources show a much larger range in values than the smooth-transition sources. If we consider only the latter sources, we get a mean of  $\langle R_{\text{dust}}/R_{\text{out}} \rangle = 1.2 \pm 0.2$  and a median value of  $R_{\text{dust}}/R_{\text{out}} = 0.95$ .

The largest source of uncertainty in our estimation of both the BELR outer radius and the hot dust radius is the black hole mass, which enters through the virial theorem in the former and the accretion disc fits in the latter. The virial black hole mass is known only within a factor of  $\sim 2-3$  (e.g. Graham et al. 2011), which translates to an uncertainty in the ratio between the two radii of a factor of  $\sim 3-5$ . Another unknown is the chemical composition of the hot dust. If we assume instead graphite dust grains and use eq. (2) of Mor & Netzer (2012), the estimated hot dust radii reduce by a factor of 1.5. Given these uncertainties, it is remarkable that for the large majority of our sample the BELR outer radius and the hot dust radius are consistent with each other within a factor of  $\lesssim 5$ . Only four sources are the exception, namely, PG 0804+761, PG 1307+085, 3C 390.3, and NGC 4593, which are all of the inflected type. Therefore, it appears that in general the BELR is dust-limited.

We can compare our results also to the lag times measured from near-IR dust reverberation programmes. Koshida et al. (2009) found that the hot dust radius in the source NGC 4151 changed between 30 and 70 days, which is a factor of  $\sim 3-6$  lower than our BELR outer radius of 181 lt-days, but consistent with our estimated hot dust radius of 89 lt-days. Suganuma et al. (2006) found a lag time of  $\sim 50$  days for the source NGC 5548, consistent with our value of the BELR outer radius of 65 lt-days, but a factor of  $\sim 6$  lower than our estimated hot dust radius of 279 lt-days. On the other hand, their lag times for the sources NGC 3227 ( $\sim 20$  days) and NGC 7469 (65–87 days) are considerably lower (by a factor of  $\sim 7$  and  $\sim 9-12$ , respectively) than our BELR outer radii. For the source NGC 7469, their lag times are also much lower (by a factor of  $\sim 7-10$ ) than our estimated hot dust radius of 620 lt-days, whereas we have no estimate of the hot dust radius for the source NGC 3227 since both its near-IR and optical spectra were found to be strongly dominated by the host galaxy starlight (Landt et al. 2011b). The fact that lag times measured by dust reverberation programmes are systematically smaller than dust radii estimated from the AGN bolometric luminosity and the dust sublimation temperature has been noted previously (Oknyanskij & Horne 2001; Kishimoto et al. 2007;

Nenkova et al. 2008). Kawaguchi & Mori (2010, 2011) ascribe this to a dust geometry that is bowl-shaped rather than spherical due to the anisotropy of the accretion disc emission. Such a geometry would place the dust further away from the continuum source but nearer to the observer for pole-on views, thus reducing the observed dust reverberation times relative to the dust radius estimated from the continuum radiation.

Netzer & Laor (1993) showed that dust strongly reduces the emissivity of the broad line gas. Then, assuming that dust is present at all distances outside the BELR, emission from the NELR will appear only at much larger radii and an obvious, large gap in velocity field between the BELR and NELR is expected. This is observed in the inflected sources, but it is not immediately clear how the smooth-transition sources can fit in this scenario. One possibility is that the ionisation parameter is smaller in the latter than in the former sources, as already suggested by our results based on Fig. 4 (upper panel). Since the effects of dust on the gas emissivity due to its absorption of ionising photons and destruction of line photons are stronger the higher the ionisation parameter, a relatively small ionisation parameter in the smooth-transition sources would mean that the dust barely affects the line emissivity thus producing only a small, unperceptible velocity gap between the BELR and NELR.

The ionisation parameter, which is defined as  $U = \Phi/(n \cdot c)$ , where  $\Phi$  is the ionising flux,  $n$  is the number density and  $c$  is the speed of light, is a measure of the number of photons available to ionise versus the number of atoms available to be ionised. Since the ionising luminosity is on average similar for the inflected and smooth-transition sources ( $\langle \log \nu L_{\text{tot}} \rangle = 45.45 \pm 0.23$  and  $46.22 \pm 0.22$ , respectively), a lower ionisation parameter in the latter would imply a line emitting gas of a higher number density. Such high-density gas is expected to produce copious emission from low-ionisation species such as, e.g., O I, Fe II, and Ca II, and this even at large distances from the ionising source. Indeed, in Landt et al. (2008), we showed that whereas the inflected sources have only broad O I emission, the O I  $\lambda 8446$  and O I  $1.1287 \mu\text{m}$  emission line profiles of the smooth-transition sources show both a broad and a narrow component.

## 5 THE GEOMETRY AND KINEMATICS

All current BELR models assume that the gas motion is dominated by the gravitational potential of the central black hole, i.e. that the gas is virialised. The differences between them lie mainly in the geometry of the gas distribution and the presence or absence of a radial component. In this section, we briefly discuss under which assumptions the most popular BELR models are able to produce a broad line profile with a flat top. In the following, we consider (i) a spherical gas distribution in orbital motion; (ii) a pure Keplerian disc; and (iii) a Keplerian disc with a wind.

A flat-topped broad line profile is produced by a spherical gas distribution in orbital motion (or in gravitational infall) if a sharp outer boundary rather than an indefinitely large outer radius is assumed. This has been noted by several authors who have calculated detailed broad line profiles from such models (e.g. Capriotti et al. 1980; Robinson et al.

1990; Robinson 1995; Corbin 1997; Korista & Goad 2004). However, the assumption of a sharp outer boundary was always considered to be artificial, since most observed broad emission line profiles were peaked. In spherical models, a flat-topped profile is expected for ratios between the BELR outer and inner radius of  $R_{\text{out}}/R_{\text{in}} \lesssim 200$ .

A pure Keplerian disc produces for most orientations and radial extents of the disc a double-horned broad emission line profile (e.g. Horne & Marsh 1986; Chen & Halpern 1989; Dumont & Collin-Souffrin 1990). The two horns are separated by velocities of  $\gtrsim 600 \text{ km s}^{-1}$ , and, therefore, a flat top is generally not expected. The only exception are profiles predicted for relatively small angles between the observer and the disc rotation axis of  $\lesssim 15^\circ$ , for which the two horns almost merge together. However, in this case the emission line width is also considerably reduced. A bowl-shaped geometry, as recently proposed by Goad et al. (2012), produces broad emission line profiles largely similar to those of a pure Keplerian disc. We note that the Balmer broad emission lines H $\alpha$  and H $\beta$  of the source 3C 390.3, which is included in our sample, have been previously modelled with a disc (Perez et al. 1988; Zheng et al. 1991; Eracleous & Halpern 1994). We observe a Pa $\alpha$  profile for 3C 390.3 that is clearly flat-topped, but a strong wing extending to very large velocities is also apparent.

Murray et al. (1995) have shown that if a wind is (radiatively) launched from a disc in Keplerian rotation, the expected broad emission line profile changes from double-horned to single-peaked, since the substantial radial velocity shear in the wind considerably increases the optical depth and so more line photons escape along directions with low projected velocity. In this model, the emission lines arise in a thin layer where the wind emerges from the disc, which means that the motion of the line emitting gas is largely dominated by gravity. Murray & Chiang (1997) show that a flat-topped broad emission line profile is produced in the disc wind model if relatively small ratios between the BELR outer and inner radius are assumed ( $R_{\text{out}}/R_{\text{in}} \lesssim 100$ ). However, the smaller the BELR outer radius, the smaller also the expected equivalent width of the emission line. The accretion disc wind model has recently been developed further by Flohic et al. (2012) and Chajet & Hall (2013) for the low- and high-ionisation emission lines, respectively. In particular the models of Flohic et al. (2012) for the Balmer emission lines show that the width of the flat top also depends on the inclination of the disc; the broadest flat tops are expected for edge-on views.

## 6 SUMMARY AND CONCLUSIONS

We have used the Paschen hydrogen emission lines of a sample of 31 type 1 AGN to show that the BELR generally has an outer boundary. The intrinsic broad emission line profile is flat-topped, which means that the BELR and NELR are kinematically separate. Our near-IR spectra, which were obtained in cross-dispersed mode at the IRTF 3 m and Gemini North 8 m observatories, have both a large wavelength coverage and a high continuum S/N ratio ( $\gtrsim 100$ ). This allowed us to study even the weakest lines in the Paschen series and to interpret the unblended profiles of the strongest Paschen



lines, Pa $\alpha$  and Pa $\beta$ , with high confidence. Our main results can be summarised as follows.

(i) The higher-order Paschen lines (in particular the Pa9 and Pa10 lines) provide observational evidence that the BELR has an outer radius. Their narrow components are absent in *all* sources, revealing a broad emission line profile that is intrinsically flat-topped. This result indicates that the BELR and NELR are kinematically separate and is most relevant for AGN with relatively narrow broad emission lines, for which the transition between the broad and narrow line components is not obvious.

(ii) We have calculated the BELR outer radius from the *half* width of the flat top in the Pa $\alpha$  or Pa $\beta$  profiles using the virial theorem. The resulting values follow a radius-luminosity relationship with a logarithmic slope of  $0.7 \pm 0.1$ , which is consistent (within  $2\sigma$ ) with the value of 0.5 expected from simple photoionisation arguments. This indicates that the BELR in all AGN ceases at a similar ionising flux.

(iii) We have estimated the dust sublimation radius from the AGN bolometric luminosity (approximated with the total accretion disc luminosity) and the hot dust temperature and find that it is on average similar to the BELR outer radius. The distribution of the ratios between the two radii has a mean of  $\langle R_{\text{dust}}/R_{\text{out}} \rangle = 1.9 \pm 0.6$ . Sources with an obvious transition between their broad and narrow line components show a much larger range in values than those with relatively narrow broad emission lines. If we consider only the latter sources, the mean moves closer to one ( $\langle R_{\text{dust}}/R_{\text{out}} \rangle = 1.2 \pm 0.2$ ). Although a dust-bounded BELR was already proposed early on (Netzer & Laor 1993), we present a firm observational evidence for it.

(iv) The observation of an intrinsically flat-topped broad emission line profile can constrain the geometry and kinematics of the BELR. Spherical models with orbital motion or infall produce a flat top if a sharp outer boundary rather than an indefinitely large outer radius is assumed. This is also the case for the accretion disc wind model of Murray et al. (1995). The required ratios between the BELR outer and inner radius in these models are  $\lesssim 100 - 200$ . On the other hand, a pure Keplerian disc produces for most orientations and radial extents of the disc a double-horned broad emission line profile.

## ACKNOWLEDGMENTS

We thank Kirk Korista and Brad Peterson for their comments on an earlier version of this manuscript. H. L. acknowledges financial support by the European Union through the COFUND scheme. This work is partly based on observations obtained at the *Gemini* Observatory, which is operated by the Association of Universities for Research in Astronomy, Inc., under a cooperative agreement with the NSF on behalf of the Gemini partnership: the National Science Foundation (United States), the Science and Technology Facilities Council (United Kingdom), the National Research Council (Canada), CONICYT (Chile), the Australian Research Council (Australia), Ministério da Ciência, Tecnologia e Inovação (Brazil) and Ministerio de Ciencia, Tecnología e Innovación Productiva (Argentina).

## REFERENCES

- Baldwin, J., Ferland, G., Korista, K., & Verner, D. 1995, ApJ, 455, L119
- Bentz, M. C., et al. 2006, ApJ, 651, 775
- Bentz, M. C., Peterson, B. M., Netzer, H., Pogge, R. W., & Vestergaard, M. 2009, ApJ, 697, 160
- Capriotti, E., Foltz, C., & Byard, P. 1980, ApJ, 241, 903
- Chajet, L. S., & Hall, P. B. 2013, MNRAS, 429, 3214
- Chen, K., & Halpern, J. P. 1989, ApJ, 344, 115
- Collin-Souffrin, S., & Lasota, J.-P. 1988, PASP, 100, 1041
- Corbin, M. R. 1997, ApJ, 485, 517
- Denney, K. D., et al. 2006, ApJ, 653, 152
- Denney, K. D., et al. 2010, ApJ, 721, 715
- Dietrich, M., et al. 2012, ApJ, 757, 53
- Dumont, A. M., & Collin-Souffrin, S. 1990, A&A, 229, 313
- Elias, J. H., Joyce, R. R., Liang, M., Muller, G. P., Hileman, E. A., & George, J. R. 2006, in Society of Photo-Optical Instrumentation Engineers (SPIE) Conference Series, Vol. 6269, Society of Photo-Optical Instrumentation Engineers (SPIE) Conference Series
- Emmering, R. T., Blandford, R. D., & Shlosman, I. 1992, ApJ, 385, 460
- Eracleous, M., & Halpern, J. P. 1994, ApJS, 90, 1
- Ferland, G. J. 2003, ARA&A, 41, 517
- Flohic, H. M. L. G., Eracleous, M., & Bogdanović, T. 2012, ApJ, 753, 133
- Goad, M. R., Korista, K. T., & Ruff, A. J. 2012, MNRAS, 426, 3086
- Graham, A. W., Onken, C. A., Athanassoula, E., & Combes, F. 2011, MNRAS, 412, 2211
- Grier, C. J., et al. 2012, ApJ, 755, 60
- Horne, K., & Marsh, T. R. 1986, MNRAS, 218, 761
- Jin, C., Ward, M., Done, C., & Gelbord, J. 2012, MNRAS, 420, 1825
- Kawaguchi, T., & Mori, M. 2010, ApJ, 724, L183
- Kawaguchi, T., & Mori, M. 2011, ApJ, 737, 105
- Kishimoto, M., Hönig, S. F., Beckert, T., & Weigelt, G. 2007, A&A, 476, 713
- Korista, K. T., & Goad, M. R. 2000, ApJ, 536, 284
- Korista, K. T., & Goad, M. R. 2004, ApJ, 606, 749
- Koshida, S., et al. 2009, ApJ, 700, L109
- Krolik, J. H., McKee, C. F., & Tarter, C. B. 1981, ApJ, 249, 422
- Landt, H., Bentz, M. C., Peterson, B. M., Elvis, M., Ward, M. J., Korista, K. T., & Karovska, M. 2011a, MNRAS, 413, L106
- Landt, H., Bentz, M. C., Ward, M. J., Elvis, M., Peterson, B. M., Korista, K. T., & Karovska, M. 2008, ApJS, 174, 282
- Landt, H., Elvis, M., Ward, M. J., Bentz, M. C., Korista, K. T., & Karovska, M. 2011b, MNRAS, 414, 218
- Landt, H., Ward, M. J., Peterson, B. M., Bentz, M. C., Elvis, M., Korista, K. T., & Karovska, M. 2013, MNRAS, 432, 113
- Marziani, P., Sulentic, J. W., Dultzin-Hacyan, D., Čalvani, M., & Moles, M. 1996, ApJS, 104, 37
- Marziani, P., Sulentic, J. W., Zamanov, R., Calvani, M., Dultzin-Hacyan, D., Bachev, R., & Zwitter, T. 2003, ApJS, 145, 199
- Mathews, W. G. 1974, ApJ, 189, 23
- Mor, R., & Netzer, H. 2012, MNRAS, 420, 526

- Murray, N., & Chiang, J. 1997, *ApJ*, 474, 91  
Murray, N., Chiang, J., Grossman, S. A., & Voit, G. M. 1995, *ApJ*, 451, 498  
Nenkova, M., Sirocky, M. M., Ivezić, Z., & Elitzur, M. 2008, *ApJ*, 685, 147  
Netzer, H., & Laor, A. 1993, *ApJ*, 404, L51  
Oknyanskij, V. L., & Horne, K. 2001, in *Astronomical Society of the Pacific Conference Series*, Vol. 224, *Probing the Physics of Active Galactic Nuclei*, ed. B. M. Peterson, R. W. Pogge, & R. S. Polidan, 149  
Osterbrock, D. E., Koski, A. T., & Phillips, M. M. 1975, *ApJ*, 197, L41  
Osterbrock, D. E., Koski, A. T., & Phillips, M. M. 1976, *ApJ*, 206, 898  
Perez, E., Mediavilla, E., Penston, M. V., Tadhunter, C., & Moles, M. 1988, *MNRAS*, 230, 353  
Peterson, B. M. 1993, *PASP*, 105, 247  
Peterson, B. M., et al. 2004, *ApJ*, 613, 682  
Rayner, J. T., Toomey, D. W., Onaka, P. M., Denault, A. J., Stahlberger, W. E., Vacca, W. D., Cushing, M. C., & Wang, S. 2003, *PASP*, 115, 362  
Robinson, A. 1995, *MNRAS*, 272, 647  
Robinson, A., Perez, E., & Binette, L. 1990, *MNRAS*, 246, 349  
Suganuma, M., et al. 2006, *ApJ*, 639, 46  
Zamfir, S., Sulentic, J. W., Marziani, P., & Dultzin, D. 2010, *MNRAS*, 403, 1759  
Zheng, W., Veilleux, S., & Grandi, S. A. 1991, *ApJ*, 381, 418

## **APPENDIX A: PASCHEN BROAD EMISSION LINE PROFILES**

This paper has been typeset from a  $\text{\LaTeX}$  file prepared by the author.

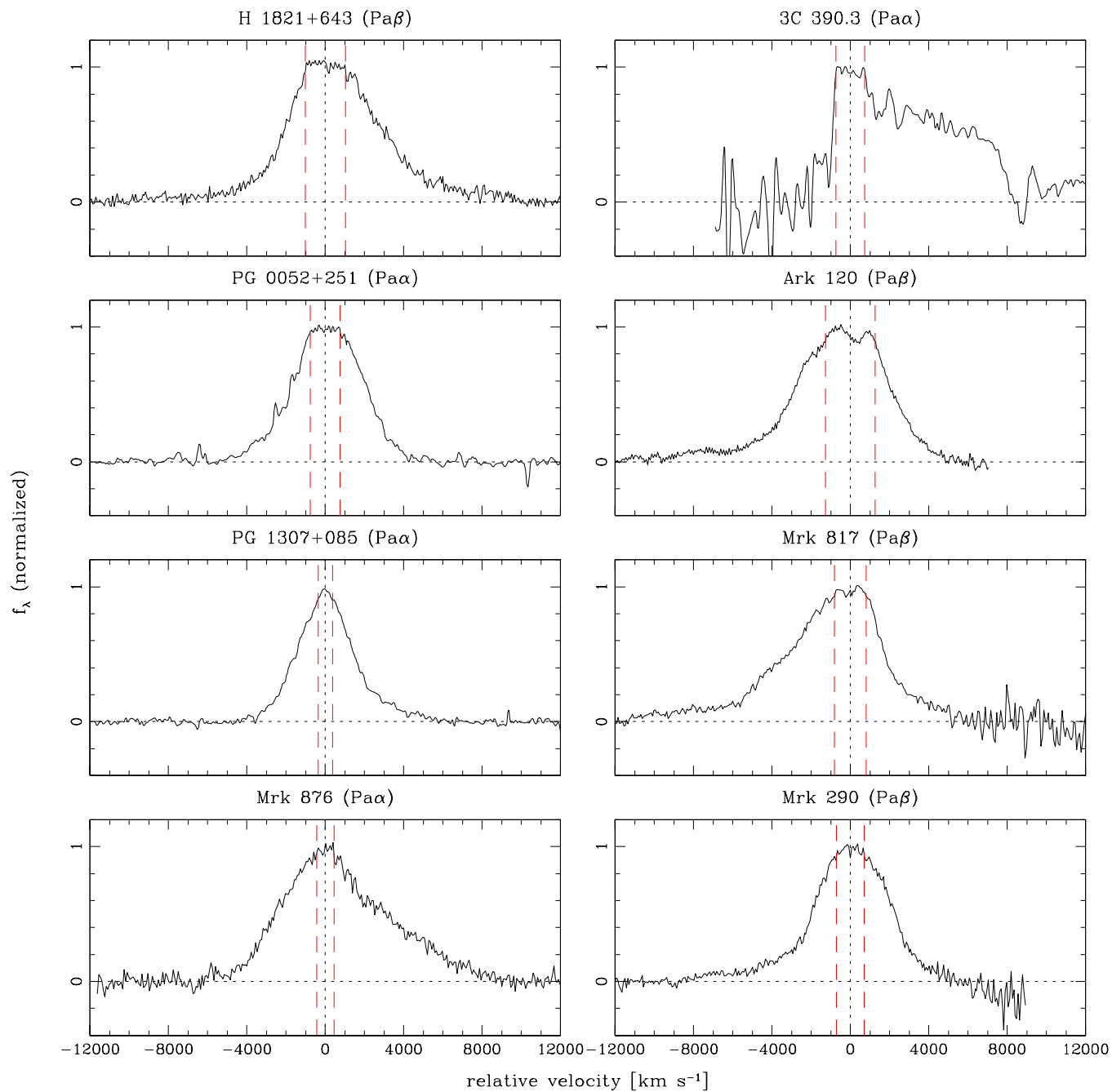


**Figure A1.** Profiles of the Pa $\alpha$  or Pa $\beta$  broad components (whichever had the higher S/N ratio) in velocity space for the inflected sources, i.e. sources with an obvious transition between the broad and narrow emission line components. The line profiles have been normalised to the same intensity of the flat top and shifted such that the flat top centre (vertical black dotted line) is at zero velocity. The two vertical red dashed lines mark the full width of the broad, flat top.

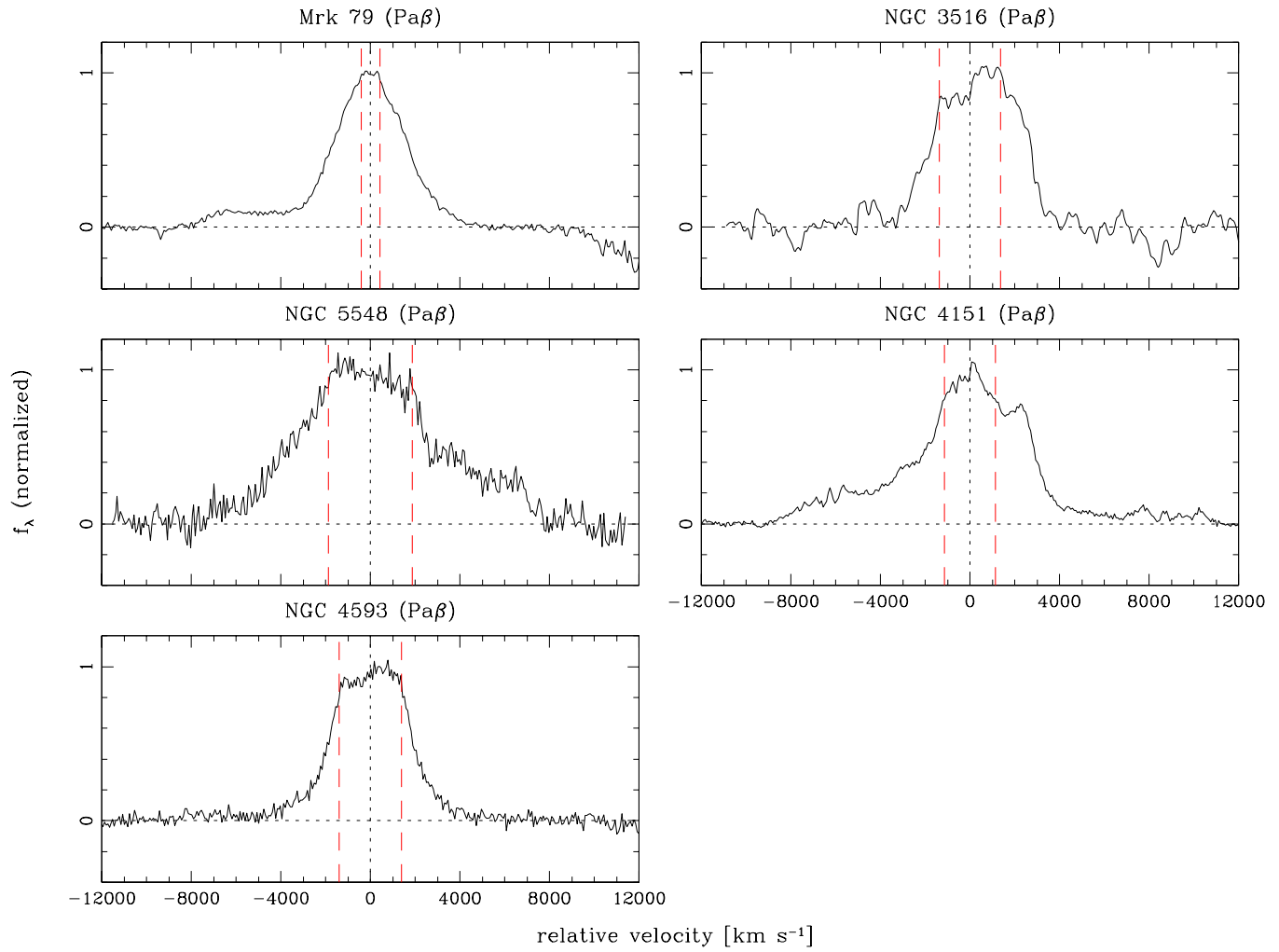


**Figure A1** – *continued*

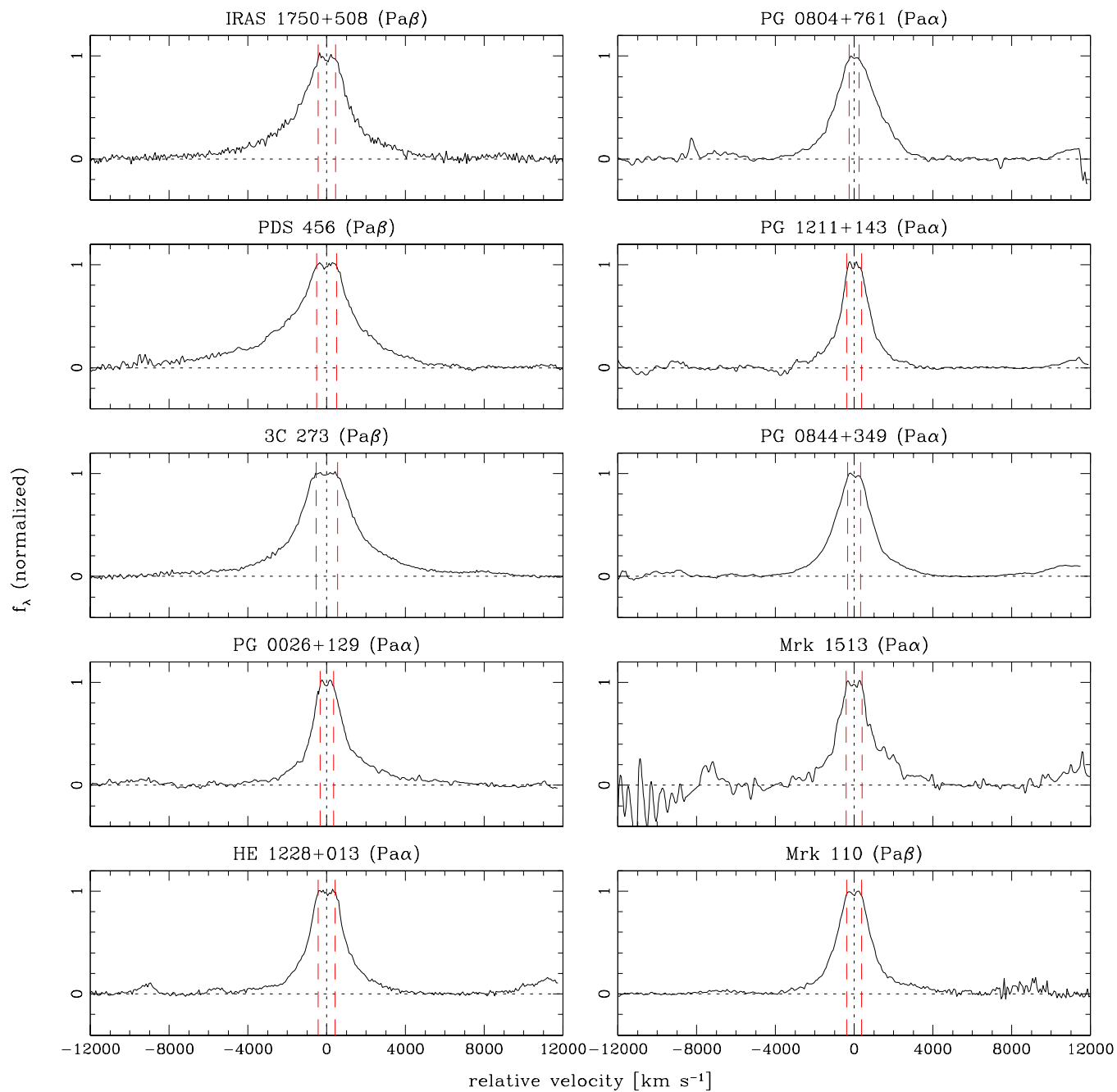


**Figure A2.** Same as in Fig. A1 for the smooth-transition sources, i.e. sources with an estimated transition between the broad and narrow emission line components. The three inflected sources 3C 120, NGC 7469 and NGC 3227 with their relatively narrow broad components have also been included.



**Figure A2** – *continued*